Impedimetric Characterization of Bioelectronic Nano-antennae

Andie J. Robinson[a], Akhil Jain[a], Ruman Rahman[b], Sidahmed Abayzeed[c], Richard J. M. Hague[d], Frankie J. Rawson[a*]*

Andie J. Robinson, Dr. Akhil Jain, Dr. Frankie J. Rawson*
Regenerative Medicine and Cellular Therapies, School of Pharmacy, University of Nottingham, Nottingham, NG7 2RD, UK
*Email: Frankie.Rawson@nottingham.ac.uk

Dr. Ruman Rahman
Children's Brain Tumour Research Centre (CBTRC), Biodiscovery Institute, School of Medicine, University of Nottingham, Nottingham, NG7 2RD, UK

Dr. Sidahmed Abayzeed*
Optics and Photonics Research Group, Faculty of Engineering, University of Nottingham, Nottingham, NG7 2RD, UK
*Email: Sidahmed.Abayzeed2@nottingham.ac.uk

Prof. Richard J. M. Hague
Centre for Additive Manufacturing, Faculty of Engineering, University of Nottingham, Nottingham, NG8 1BB, UK

Keywords: impedance spectroscopy, gold nanoparticles, bioelectronics, bipolar electrochemistry

The merging of electronics with biology at the nanoscale holds considerable promise for sensing and modulating cellular behavior. Advancing our understanding of nano-bioelectronics will facilitate development and enable applications in biosensing, tissue engineering and bioelectronic medicine. However, studies investigating the electrical effects when merging wireless conductive nanoelectrodes with biology are lacking. Consequently, a new tool is required to develop a greater understanding of the bioelectrical effects of merging conductive nanoparticles with biology. Herein, this

challenge is addressed by developing an impedimetric method to evaluate bipolar electrochemical systems (BESs) that could act as nano-antennas. A theoretical framework is provided, using impedance to determine if conductive nanoparticles can be polarized and used to drive current. It is then demonstrated that 125 nm Au nanoparticle bipolar electrodes (BPEs) could be sensed with biology when incorporated extracellularly. These results highlight how nanoscale BPEs act in biology and characterize their behavior in electric fields. This research will impact on the rational design of using BPE systems in biology for both sensing and actuating applications.

1. Introduction

We are entering a new era where bioelectronic tools enable us to harness and modulate cellular electricity. This allows us to control and sense cell behavior for various applications, from biosensing[1], microbial fuel cells[2] and to the treatment of disease.[3] One of the remaining challenges to be overcome to further advance this area is to develop new nano-bioelectronics, capable of interfacing with cells at an equivalent spatial level of cellular electronic components, which can be operated remotely in a non-invasive manner. Also, key is the development of new sensing systems capable of measuring cellular bioelectronic inputs and outputs. In doing so, this will shed light on how bioelectricity underpins cell behavior. To date, the rational design of wireless nano-bioelectronic systems has been limited due to the lack of label-free analytical techniques to study electrical effects on conductive nano-sized objects when combined with cells. Therefore, one of the aims of this work was to address this particular scientific challenge and to further explore how electric fields interact with nanoscale bioelectronic systems (**Figure 1**).

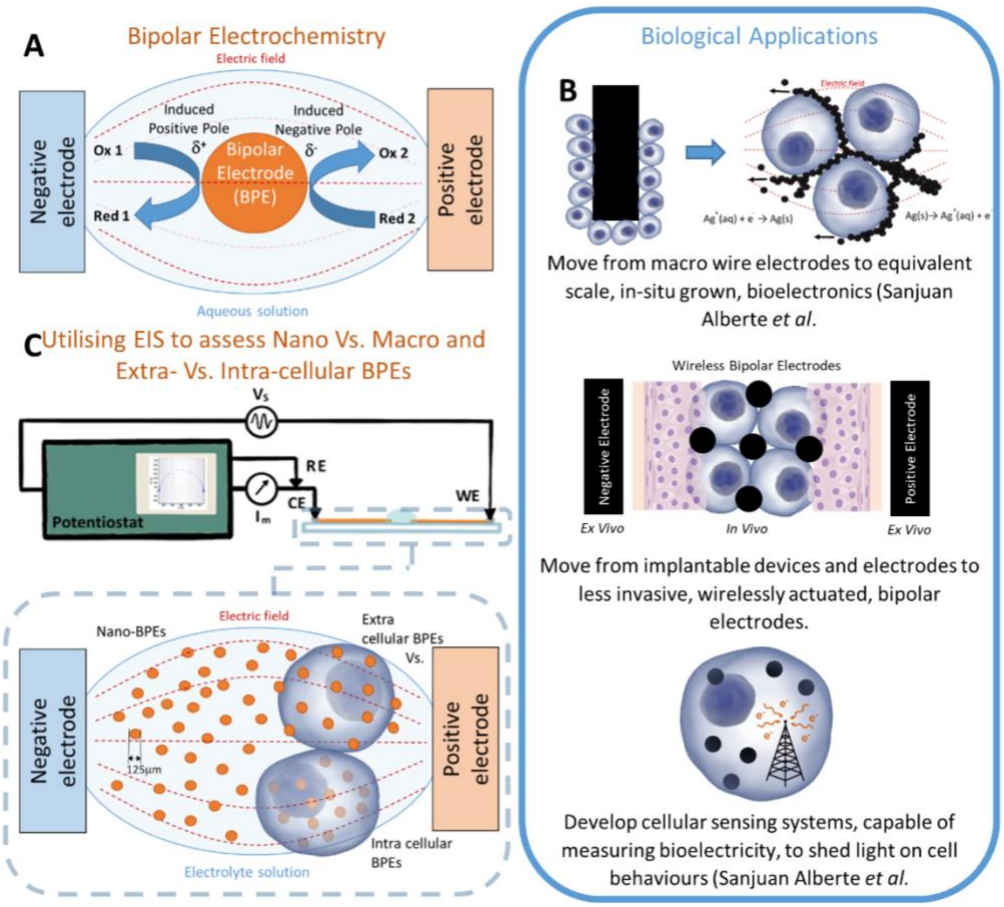

Figure 1. *Schematic showing a bipolar electrochemical cell (A), Applications of optimizing bipolar electrochemistry in vivo (B) and the experimental set-up used herein to evaluate nano-bioelectronic systems (C).*

We have recently reported on the development of a nano-bioelectronic system which was based on using nano-bipolar electrodes (nano-BPEs) in the presence of biological cells for the first time[4]. This work was based on a 'bipolar electrochemical system' (BES) which, consists of bipolar electrodes (BPEs) and an aqueous electrolyte solution.[5–8] Upon the application of an external electric field, from feeder electrodes (FEs), the bipolar electrode (BPE) becomes polarized. This means they have an induced positive and negative pole. This generates free energy that results in the ability to mediate redox reactions (Figure 1A). This ability to control redox reactions in cells has the potential for considerable therapeutic impact in diverse fields (Figure 1B). We demonstrate in this work that Au nanoparticles (AuNPs) act

as nano-antennae, due to an ability to sense external electric fields and then act as reporters via changes in electronic properties, which we sense by impedance spectroscopy (Figure 1C).

The use of BPEs in electrochemistry is widespread.[9–15] Over the last decade, new interest has revitalized the field with exciting applications at the micro/nanoscale.[16–20] However, the field has been largely neglected for cellular applications and recent conflicting observations, at the nanoscale, raises questions about the underpinning theory. For example, previously the assertion was that to polarize nanoscale BPEs, a relatively high voltage was required in the kV region[21]. However, most recent research has indicated that nano-antennae that act as bipolar electrodes are affected at much lower voltages (~10 v).[4] It is therefore clear that a further understanding of bipolar electrode characteristics is required to optimize applications at the nanoscale and within biological systems. This previous body of work demonstrated the use of direct current to wirelessly drive current at an intracellular BPE. We believe moving towards using alternating current could allow for better prospects of merging with biology due to the greater flexibility in tuning potentials by altering frequencies. Hence, the work here-in aims to better understand the effect of alternating current on BESs.

Other approaches exist to understand BPEs and optimize their use by facilitating carefully designed criteria to allow current flow through the BPEs. One approach includes equivalent circuit modelling using data from split BPEs or bespoke bipolar cells.[22–24] Translating these methods to the nanoscale would be extremely difficult, due to the need to manufacture electronics to connect to individual nano-BPEs. Another possible method is electrochemically-modulated fluorescent probes.[25] However, as this is an indirect method it is difficult to produce quantitative information and only bipolar electrodes are analyzed, thus neglecting other cell elements (electrolyte/feeder electrodes). This approach also adds the process of fluorescently tagging electrodes and typical fluorescence imaging issues such as photobleaching and subsequent irreversibility. Hence, an alternative analytical method is required that can be easily applied to nano scale bipolar electrochemical systems. We

hypothesized that Electrochemical Impedance Spectroscopy (EIS) would be suitable for studying the electrical components of nano-BPE systems as it allows for the assessment of a BES in terms of its electrical circuit behavior, without the need for physical connections to each component in the system.

EIS is a powerful tool capable of deconstructing total impedance into its capacitive, resistive and inductive contributions,[26] and has been extensively used to study corrosion.[27] Other applications include material characterization,[28,29] battery and fuel cell development[30–32] and bipolar membrane characterization.[33] In more recent years the tool has drawn interest in the life sciences field due to its ability to reveal electrochemical properties such as diffusion coefficients, electron transfer rate constants, adsorption mechanisms and charge transfer resistances.[34] These applications are dominated by EIS based biosensors, for example for label-free sensing of DNA[35] and tuberculosis,[36] possible identification of osteoporosis,[37] and identification of thyroid cancer using EoN (EIS on a needle).[38,39] EIS has also been widely applied to living cells in order to non-invasively count, identify or monitor cellular functions,[40] state-of-the-art instrumentation is now available allowing the monitoring of cell adhesion, morphology, proliferation, and motion of cells (electrical cell-substrate impedance sensing – ECIS®).[41] EIS is extremely practical and easy to carry out, whilst also being quickly repeatable. As seen by the wide array of applications, this makes EIS an attractive technique for analytical purposes. Importantly, to the best of our knowledge, it has not been used to study cellular electrochemical systems as proposed here (Figure 1).

Herein, we report on a label-free EIS tool for direct modelling of the equivalent circuits of BESs. As seen in Figure 1C, this was performed using 125 nm AuNP BPEs, in electrolytes including water and phosphate-buffered saline (PBS). These nano-BPEs were then combined with biological systems to establish if they could act as bipolar nano-antennae with cells. The developed assay sheds light on how electrical input behaves with biology when using bipolar electrodes as electrical antennae. This indicates that electrical input parameters can be tuned to

drive electrical polarization of nanoparticles, which could be used to design systems to manipulate cellular biochemistry in a wireless manner.

2. Results and Discussion

Our first step in designing an analytical tool that could be used to help us understand how bipolar electrodes behave under an electric field was to model them using a simplified equivalent circuit with three circuit elements. These elements are the impedance of the feeder electrodes (Z_F), the impedance of the bipolar electrodes (Z_B) and the 'bypass impedance' of the electrolyte (Z_E). **Figure 2** (inset) shows the configuration of these components for samples with BPEs, without cells.

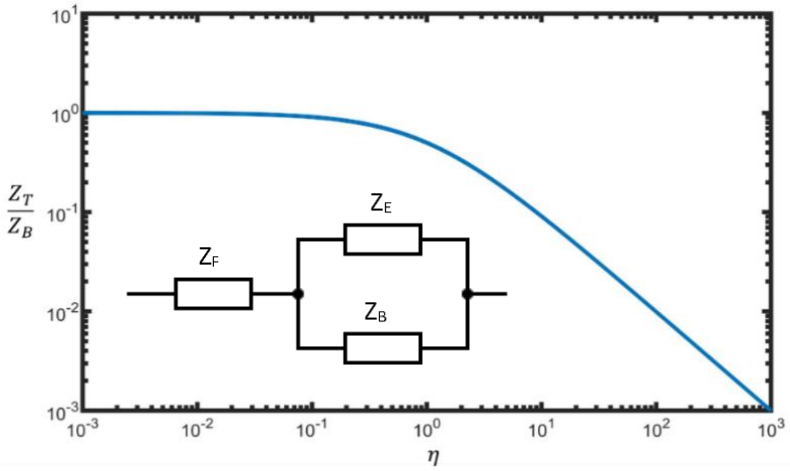

Figure 2. *Basis of EIS method to evaluate bipolar electrochemical systems, by evaluating the ratio of BPE impedance and electrolyte impedance. Total impedance, normalized by BPE impedance, is plotted against efficiency parameter η (defined in Equation 1). Equivalent Circuit can be seen inset, with impedance components relating to the feeder electrodes Z_F, the electrolyte Z_E, and the bipolar electrodes Z_B.*

An impedance-based parameter was then introduced with the ability to quantitatively-describe the efficiency of these BESs in driving current. η is defined as the ratio of the impedance of the bipolar electrodes (Z_B) to the bypass impedance of the electrolyte (Z_E), as described by (Equation 1). This parameter does not include the impedance of the feeder

electrode (Z_F) as its effect on the overall cell impedance is negligible, exerting a low impedance in series with the overall impedance of the bipolar system.

$$\eta = \frac{Z_B}{Z_E} \quad (1)$$

$$Z_T = \frac{Z_E Z_B}{Z_E + Z_B} \quad (2)$$

In order to investigate the influence of the efficiency parameter on the total cell impedance, we can model a BES with a fixed Z_B and varying Z_E. As seen in Figure 2, by calculating total impedance (Z_T), using Equation 2, and normalizing using Z_B, we can plot normalized total impedance against the efficiency parameter, giving three distinct regions of η.

In the range where $\eta \geq 10$, Z_T is dominated by Z_E; this case occurs when a highly conductive electrolyte is used. Current will favor the electrolyte, meaning little to no current would pass through the BPEs, therefore being undesirable in driving electrochemical reactions. As Z_E increases, to then fall within the range of $0.1 < \eta < 10$, Z_T begins to reflect both Z_E and Z_B. This is due to impedance values becoming more similar and hence current tends towards equally splitting between the two components. Finally, when η falls below 0.1, the overall impedance is then limited only by Z_B. This shows that when a highly resistive electrolyte is used, current would then favor the BPEs with little to no current passing through the electrolyte. In order to drive electrochemical reactions at the BPE, and to probe any changes in the BPEs, current is required to pass through the BPEs. Hence, we can conclude that $\eta \leq 10$ must be satisfied when using this analytical method. A similar concept has previously been described, though not using impedance spectroscopy as in this study[21]. Previous studies required physical connection or labelling of the bipolar electrodes to assess electrical behavior of BPEs[22,24,25]. Utilizing impedance spectroscopy is label-free and therefore allows a much simpler method, but also allows for the analysis of nano-BPEs for the first time.

2.1. Nano BPE systems

Before exploring how BESs behave in the presence of cells, we first validated the above theoretical framework with FEs, BPEs and varying electrolytes only. The BES consisted of gold feeder electrodes with spherical gold nanoparticle (AuNP) BPEs placed in between. AuNP BPEs are commonly used for *in vivo* applications.[42] Furthermore, we have recently developed bioelectronic systems using AuNPs in which we observed they could act as electrical antennae within cells[4]. They would, therefore, be suitable for establishing an EIS analytical protocol to study the effects of nano-sized bipolar electrodes in biology. A larger diameter particle is used here-in (125 nm) to allow for higher charge density and compatibility with other techniques, such as assessing plasmonic effects.[4] In order to test the effect of varying Z_E and hence experimentally validate the above model (Figure 2), samples were tested in high and low impedance electrolytes: deionized water and PBS respectively. Furthermore, a range of concentrations of PBS were also studied to further confirm the hypothesis that increasing Z_E allows for the increased efficiency of the system (η) (Figure S1). It is important to note that this is not to simulate *in vivo* conditions, but to assess how these nano BESs behave in high and low impedance electrolyte examples.

Subsequently, we then analyzed the resulting frequency impedance plots by least squared fitting to construct equivalent circuits (**Figure 3**). Warburg impedance was also included in series with the feeder electrode to account for diffusion in the system and allow for better fitting. However, it was found that these values were not significantly different between repeats and hence are not discussed. All results did satisfy the Kronig-Kramer's test, showing that the system is linear and stable with time, which is a pre-requisite for circuit modelling. Both FEs and BPEs are adequately described by a capacitor only, in the absence of charge transfer across the interface, therefore $Z_{F/B}$ are modelled as $C_{F/B}$. When deionized water is used as an electrolyte, the impedance of AuNPs is lower in comparison to Z_E, resulting in current flow through the BPEs. The current passes through BPEs capacitively, therefore an additional capacitor appears in the equivalent circuit accounting for this effect (Figure 3A). In contrast to

deionized water, when PBS is used current flows through the electrolyte, the impedance of BPEs is relatively high and therefore behaves as an open circuit (Figure 3B). As PBS is more physiologically relevant to intra/extracellular space than deionized water, BPE concentration and position will be extremely important in order to drive current in the presence of cells. Because of the practicality of this method, equivalent circuits are much easier to produce from a practical standpoint when compared to previous methods for probing BPEs[22–24].

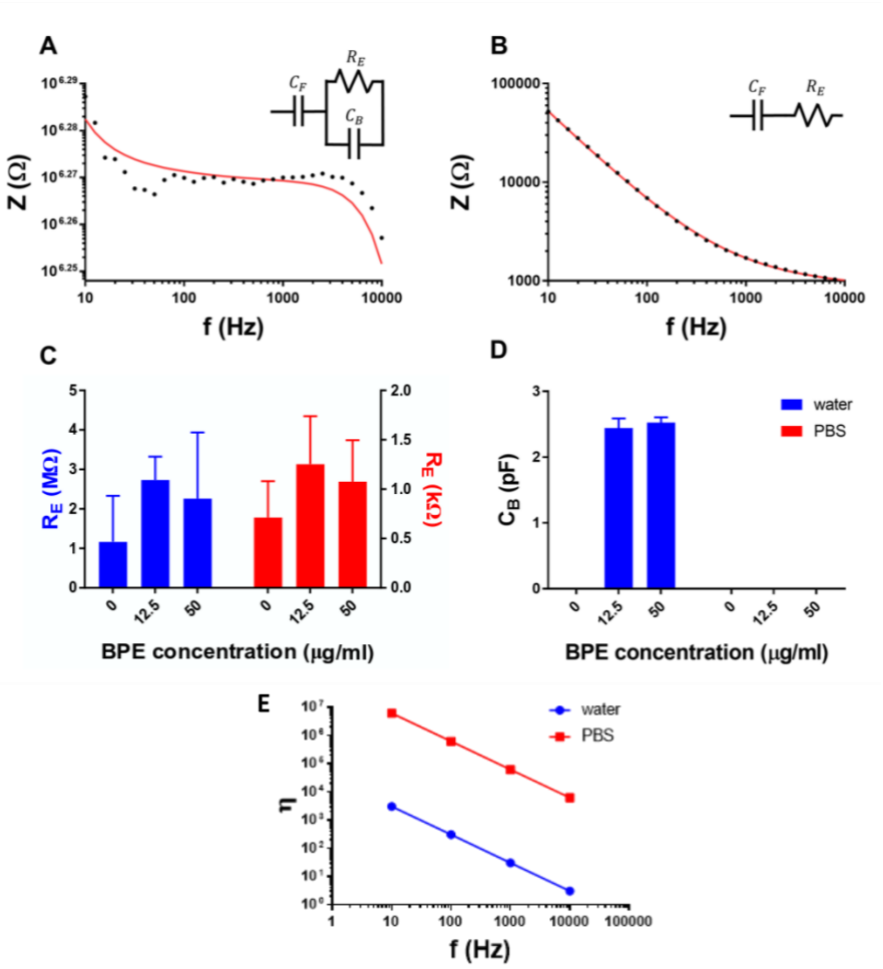

Figure 3. *Example circuit fittings of Au feeder electrodes with AuNP bipolar electrodes in water (A) and PBS (B). Circuit diagrams can be seen in the inset. Warburg impedance was also included in series with the feeder electrode to account for diffusion in the system and allow for better fitting. With Z_E being modelled as a resistor (R_E) and Z_B modelled as a capacitor (C_B), C and D show the average magnitudes of R_E and C_B respectively. Error bars show standard error of mean (n = 3). Efficiency parameter (η) of 125 nm AuNP BPEs in PBS (blue) and deionized water (red) can be seen in E.*

Bode plots shown in Figure 3A and 3B for deionized water and PBS respectively, confirm that the BESs do behave differently with varying electrolyte impedance. Within the water, there are three distinct sections of the impedance spectrum. At low frequencies, the impedance is limited by the capacitive nature of the feeder electrodes. This shows a typical frequency dependent behavior, described in Equation 3, where impedance drops by increasing frequency. The second region is characterized by a constant impedance occurring within the frequency range ~100 - 3000 Hz. This component arises from the resistance of charge flow (i.e. Z_E, electrolyte impedance). When this is described in terms of the theoretical framework, previously described in Figure 2, the parameter $\eta \geq 10$ for this region. This means, within this region, the electrolyte impedance is still relatively lower than the BPE impedance and therefore is limiting the overall impedance. As the BPE is also behaving as a capacitor, its impedance is also frequency-dependent; hence, the impedance of the BPEs becomes less than the impedance of the electrolyte for the frequency range 3000 – 10,000 Hz. This means current flows through the BPE when $\eta \leq 10$ is fulfilled. It can therefore be concluded that in order to probe these nano-BPEs using impedance spectroscopy, within deionized water, measurements should be performed at frequencies higher than ~3000 Hz when relatively low voltages are applied. However, it is worth noting that there is a possibility of driving current at low frequencies if higher voltages are applied as we have observed previously.[4] Within PBS, Figure 3B, we only observe two disparate sections of the curve relating to (i) the capacitive effect of the FEs at lower frequencies; and (ii) plateauing to the resistive effect of the electrolyte at high frequencies. As expected, the addition of BPEs does not significantly change the impedance spectra, indicating we are working within the region of $\eta \geq 10$ with little to no current flowing through the BPEs. As within deionized water, it is expected that at much higher frequencies the BPEs may then be able to be sensed due to their decreasing impedance.

$$Z = \frac{1}{j\omega c}$$

$$where\ \mathrm{j} = \sqrt{-1}, \omega = \text{angular frequency or } 2\pi\mathrm{f} \text{ and } \mathrm{c} = \text{capacitance} \quad (3)$$

We were then interested in determining how the different BES components are behaving, which would yield knowledge to better understand and design systems. The average of the equivalent circuit components from three independent repeats is plotted in Figure 3C and D. These plots present the electrolyte resistance (R_E) and the BPE capacitance (C_B) respectively. Feeder electrode behavior is not discussed here as it has low impedance in series with the BES and does not affect the BPEs. As seen in Figure 3C, the resistance of deionized water is in the order of MΩ, as expected due to the low concentration of ions, and PBS impedance is in the order of kΩ. The results presented show that the electrolyte impedance is not affected by the presence or absence of the bipolar electrodes. This observation further confirms the robustness of the technique in extracting the components of the BES. As anticipated from the theoretical framework in Figure 2, the BPEs are detected in the deionized water, rather than in PBS as presented in Figure 3D. The BPE component was not included when modeling samples in PBS and with no nano-BPEs, due to markedly better fitting being achieved (this can be seen in Figure S2). AuNP BPEs were used in two concentrations to determine if the method was sensitive to such differences: 50 μg/ml and 12.5 μg/ml. The apparent difference between these concentrations is pertinent in cellular assays discussed in the following section.

Given the capacitance of BPEs calculated from equivalent circuits in Figure 3 (~2.5 pF), we then calculated the efficiency of these BPEs in different electrolyte systems by calculating η (using Equation 1 and Equation 3). It is important to note that the capacitance of the BPEs would change in PBS and an estimate of this value was not possible due to no current flowing through the BPEs. However, when applying Equation 1 and Equation 3, even a magnitude difference in capacitance will have little effect on η, therefore this will allow a rudimentary comparison between water and PBS. This comparison, seen in Figure 3E, shows that η falls

below 10 when in the water at frequencies higher than ~3000 Hz, again suggesting that we are able to drive current through these BPEs under these conditions and not when using PBS.

2.2. Living Cells with Nano BPEs

Development of bioelectronic systems that use conductive nanoparticles, to sense and actuate cellular behavior would be an extremely important advancement for cancer treatment.[43,44] Consequently, we used the assay to study how AuNP BPEs behave when placed with U251 malignant brain cancer cells. To determine whether current would flow through BPEs when cells are present, U251 cells were seeded onto samples without nano-BPEs, as well as with intracellular or extracellular nano-BPEs. Again, high and low impedance electrolytes of water and PBS respectively, were used. We have previously shown that the short time frame of these experiments using water does not affect cell viability.[45]

To provide intracellular nano-BPEs, cells were incubated with AuNPs, before seeding cells onto feeder electrodes. As seen in **Figure 5**, cellular uptake of AuNPs was confirmed using confocal microscopy. To achieve this, we covalently conjugated fluorescent Zinc(II) 5-(4-aminophenyl)-10,15,20-(tri-4-sulfonatophenyl)porphyrin triammonium (zinc porphyrin) to these AuNPs (Figure S3). For comparison purposes, two concentrations of AuNPs were tested along with two incubation times: 50 or 25 μg/ml and 6 or 24 hours. Both the higher concentration (50 μg/ml) and the longer time frame (24 h) showed significantly higher AuNPs inside cells and hence, 50 μg/ml for 24 hours was used for experiments herein. We also performed inductively coupled plasma mass spectroscopy (ICP-MS) for cellular uptake analysis of AuNPs, to support the obtained confocal data (Figure S4). Considering both confocal imaging and ICP-MS results, using porphyrin functionalized and bare AuNPs respectively, we can be confident that AuNPs are being up-taken by the cells.

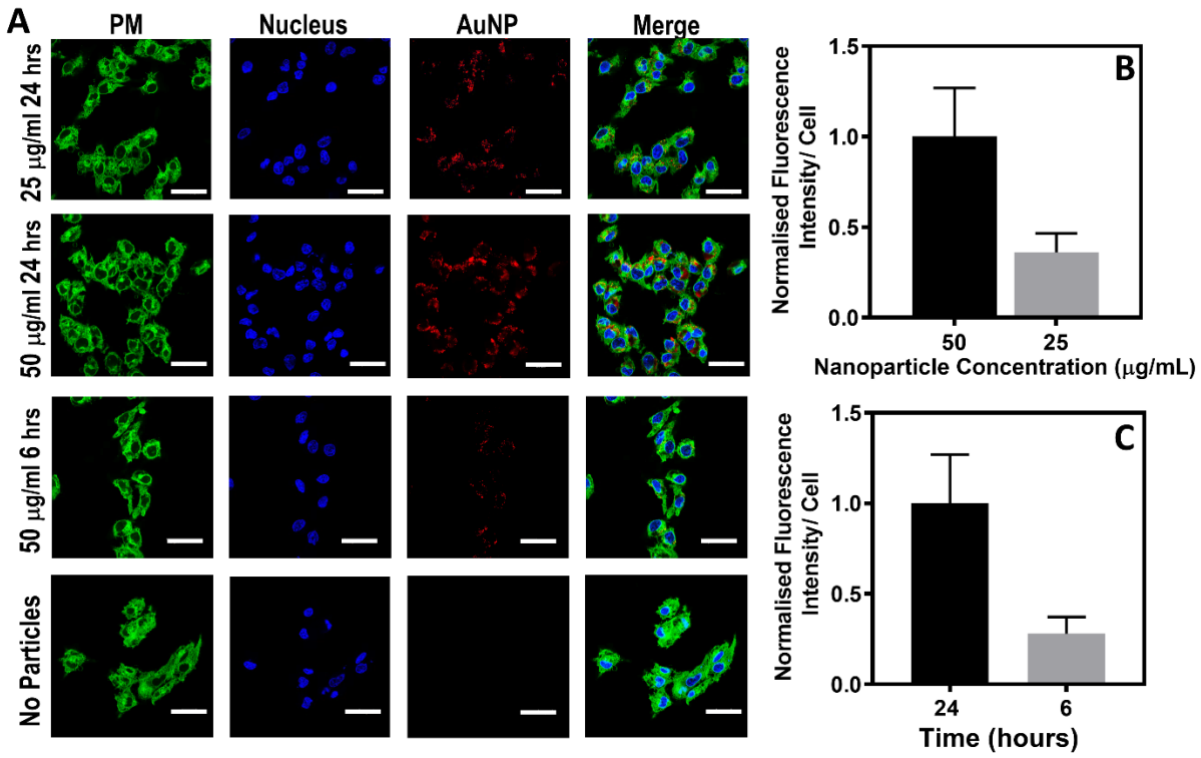

Figure 5. *Cellular uptake analysis of AuNP BPEs comparing two concentrations of AuNPs and two incubation times. Confocal microscopy was used to image U251 cells incubated with AuNPs conjugated with Zn porphyrin (A). All scale bars represent 50 µm. Mean cell fluorescent intensity as a functions of cellular uptake and SD was plotted of at least 20 cells (B and C). All the values were normalized with fluorescent intensity obtained with AuNP concentration of 50 µg/ml (B) or AuNP incubation time of 24 hours (C). 50 µg/ml AuNP concentration was taken forward from B to perform incubation time study in C.*

Cell experiments were initially performed between the frequencies of 10 - 10,000 Hz and a current limit of 1 mA. Introducing living cells produced a non-stable system within this range, due to the system changing over time. Due to this, the systems did not pass Kronig-Kramer's tests and cannot be reliably fitted to electrical circuits. We include this data as it is an important example of design rules when analyzing nanoparticle effects and without analyzing higher frequencies, data can be misunderstood.

As seen in **Figure 6**A, the inclusion of cells reduces the impedance of the system in both deionized water and PBS. When nano-BPEs are included extracellularly, there appears to be no

difference in impedance spectra in comparison to cells alone, with both starting at ~60 kΩ and following the same trend (Figure 6A). This suggests that within these frequencies no current is flowing through the nano-BPEs, which therefore have no effect on the overall impedance. If this were the case *in vivo*, such nano-BPEs could not be used as electrical antennae or to drive bipolar electrochemistry. As seen in Figure 6B, intracellular nano-BPEs appear to show a difference from cells alone, increasing to > 100 kΩ. However, without being able to fit equivalent circuits we are unable to investigate whether this is in fact due to nano-BPEs being sensed.

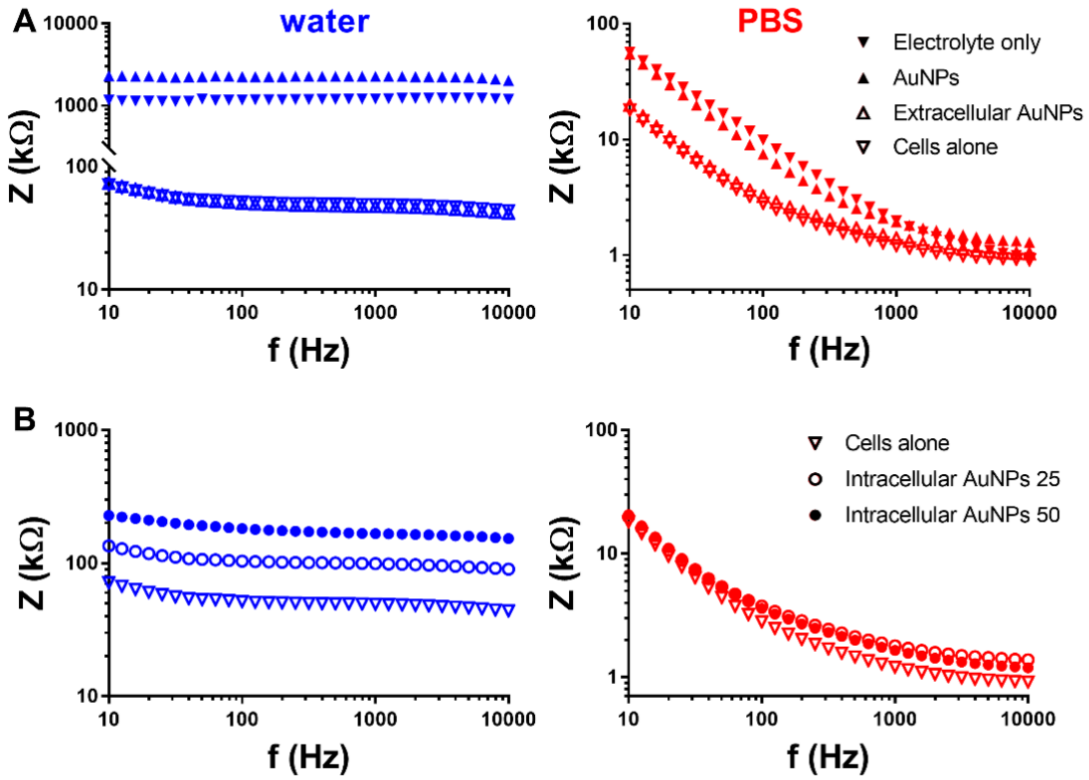

Figure 6. *Extracellular (A) and Intracellular (B) BPE impedance spectra, in water and PBS, in comparison with cells alone. Also included in A are results from the previous section: Electrolyte only and AuNPs, which consisted of AuNPs attached to the glass substrate with the addition of an electrolyte. Intracellular BPEs were incorporated in two different concentrations 25 and 50 μg/ml.*

Despite EIS being applied to many biological applications, to the best of our knowledge only one previous study exists comparing the impedance of tissue with and without the presence

of conductive objects (AuNPs).[46] As measurements are also taken at low frequencies, circuits are not fitted, so the behavior of such AuNPs cannot be quantified. Therefore, to better understand how the individual components in the systems are behaving, impedance measurements were taken covering a higher frequency range of 0.1 - 10 × 10_6 Hz. This fully covers the range of frequencies usually used to study cells using ECIS[47] and allowed us to fit circuits to better explain the systems. Furthermore, the higher frequencies are believed to be more affected by cell membranes, whereas lower frequencies are more affected by solution channels under and between adjacent cells.[48] Therefore, there is better scope to probe intracellular BPEs at these higher frequencies. Moreover, unlike raw spectra, resistance and capacitance values from fitting are normally distributed, passing a Shapiro-Wilk normality test ($p > 0.01$), allowing us to discern significant differences more easily. As low frequency did not appear to show differences between the two concentrations of AuNPs, the higher concentration was chosen to be studied at high frequencies (50 μg/ml).

As seen in **Figure 7**, to aid our interpretation a simplified circuit was suggested for cell set up which included FE capacitance (C_F), electrolyte resistance (R_E), and a new component C_T. We deem C_T to be a component that models the interaction between nano-BPEs and cells. By modelling the interactions as one single component, we assessed the differences of C_T to determine if nano-BPEs were being sensed. This simple circuit was fitted to experimental data and C_T and R_E values were plotted (Figure 7A). Sample fitting can be seen in Figure S5. With multiple cells across a square area, it is expected that the capacitance value would be similar to the capacitance value of a single cell. With this in mind, C_T values are plausible as they fit with previous cell membrane capacitance values, in the region of 10 pf[49].

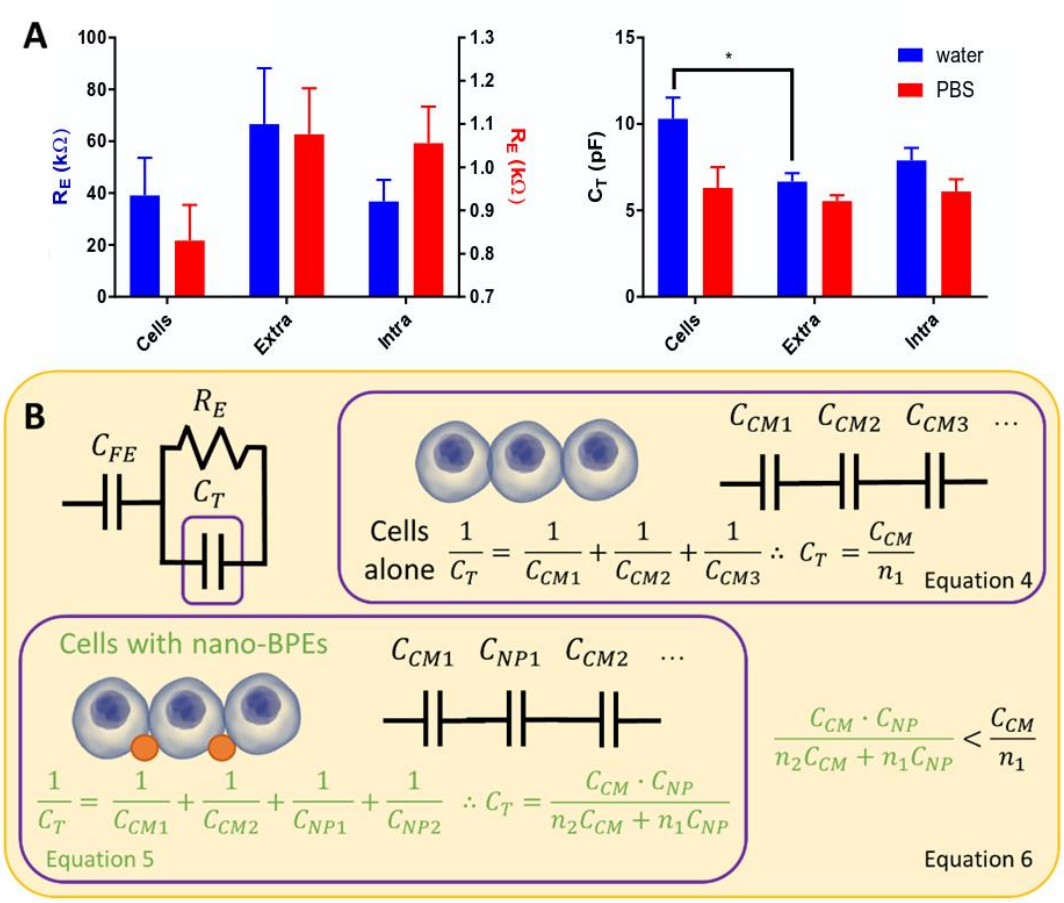

Figure 7. *Capacitance and Resistance values from circuit fittings of experimental data, with and without the presence of nano-BPEs (A). Statistical significance was shown using Sidak's multiple comparison test ($p < 0.05$). The simplified equivalent circuit fitted in A can be seen in B, along with total capacitance C_T calculations for cells alone, Equation 4, and cells with nano-BPEs, Equation 5.*

Comparing cells alone to extracellular nano-BPEs there was a significant decrease in capacitance of systems with extracellular BPEs (Figure 7A). This suggests we are driving current through these BPEs. Our initial hypothesis stated that this change in C_T could be explained by the way nano-BPEs and cells are arranged when compared to cells alone (Equation 4). This is due to series connections between nano-BPEs and cells leading to a lower capacitance than both the C_{CM} and C_{NP}, due to Equation 5. This observation suggests that extracellular interfacing, using AuNPs, reduces the dielectric properties of the cell membrane and the overall polarizability of the individual cells. This may be linked to previously explained polarization effects on membrane perturbations and conductive nano-objects.[50,51] However, more work is required to elucidate the exact physical effect. This also suggests that proposed

impedimetric characterization can be used to detect cell-nanoparticle interfacing and probe the flow of therapeutic current through these BPEs.

As seen in Figure 7A, there was no significant difference between cells alone and intracellular BPEs. This could be due to these frequencies not being high enough to penetrate through the cell membrane (not in the MHz range[52]), and so the BPEs have no effect on the impedance of the system. Despite no significant difference, there was still a reduction in mean C_T. We tentatively suggest this was due to nano-BPEs that may attach to the cell membrane that were not fully uptaken and hence, are behaving as extracellular nano-BPEs. Although this suggests no current is driven through intracellular nano-BPEs, it is possible that higher frequencies, or the application of a higher voltage could change this outcome and allow for functionality of intracellular BPEs.

These results show that, within these condition, nano-BPEs can behave as nano-antennae when in the extracellular space *in vitro*. This could have useful sensing applications. Other approaches exist that may allow us to see similar interesting effects in physiological conditions. For example using higher electrode concentrations, or higher voltages or applying similar approaches used in industry to mitigate problems associated with bypass currents.[53] This could then allow for the use of nano-BPEs in targeting or enhancing electric fields and growing *in vivo* electronics (Figure 1B i and ii). Higher frequencies, higher BPE concentrations or higher (yet still physiologically safe) voltages than used herein, may also allow for current to be driven though intracellular nano-BPEs to allow them to be used to wirelessly sense or actuate cellular functions (Figure 1B iii).

3. Conclusion

This work provides advancing knowledge on the application of nanoscale BPE systems in biology, which until now was lacking. As applied herein, EIS allows a simple way to evaluate a bipolar electrode system and model its equivalent circuit. Such a method is both simpler than existing methods[22–25] as well as possible with nano-BPEs for the first time.

Here we propose an impedimetric method of evaluating the efficiency of a bipolar electrode and electrolyte combination. By modelling total impedance in relation to BPE and electrolyte impedance, we propose the efficiency term η. We then validate this model experimentally using AuNP BPEs and high and low impedance electrolytes: deionized water and PBS respectively. This confirms that within these conditions, these BPEs can be probed in water at high frequencies, but not in PBS.

Further to this, we introduced cells to the system to aid in determining if AuNP BPEs can be used as bioelectronic antennae. The addition of cells reduces the impedance of the system in both water and PBS and provides an unstable system. To combat this, high frequency measurements were taken to allow for circuit fittings. Within this system, extracellular BPEs show a significant difference from cells alone, suggesting that current is being driven through them. Intracellular BPEs show no significant difference from cells alone, suggesting that no current is being driven though them. This is a key finding suggesting that nano-BPEs could be used as nano-antennae with biology when in the extracellular space, *in vitro*. Higher frequencies, higher BPE concentrations or higher applied voltages could potentially allow for intracellular BPEs to also drive current. Further measurements of BPEs behavior *in vivo* are required to determine whether they may be used for bioelectronics purposes.

4. Experimental Section

Electrode Manufacture: All electrodes were manufactured in house. Feeder electrodes were fabricated using a Peltier cooled dual-target sputter coater (Emitech k575x) and 3D printed polylactic acid (PLA) masks (printed using an Ultimaker). All sputter coating consisted of first coating with 20 nm of ITO (at 30 mA), as an adhesion layer, before coating with 100 nm (at 120 mA) of gold. Accurate™ spherical citrate stabilized gold nanoparticles (AuNPs) were purchased from Nano Partz™ with a diameter of 125 nm. Nano bipolar electrodes were prepared using an electrostatic coating of AuNPs in between the feeder electrodes at two

concentrations: 50 and 12.5 μg/ml. Firstly 20 μl of potassium hydroxide solution (1 M KOH in 60% ethanol) was pipetted between feeder electrodes and left for 1 hour. Following this step, two synthetic polymers with opposite charge, Poly (allylamine hydrochloride) (PAH) and Poly (sodium 4-styrenesulfnate) (PSS), were deposited for 30 minutes each. Polymer solutions were both 0.1 M in dH_2O. Finally 20 μl of AuNPs was left to drop coat overnight. Between all steps, the electrodes were washed with dH_2O and dried with nitrogen.

EIS Measurements: All impedance measurements were carried out using an Autolab potentiostat (Metrohm) in potentiostatic mode. A two-electrode system was used, with working electrode and reference/counter electrodes combined. Impedance was measured between 10 and 10,000 Hz, with a current limit set at 1mA. For high frequency measurements a high frequency module, attached to the potentiostat, was used (EC100). Ag conductive paint (RS components) was used to create larger contact areas to attach samples to the potentiostat via crocodile clips. A single droplet of 20 μl of electrolyte was used to bridge the gap between feeder electrodes.

Surface Functionalization of Gold Nanoparticles: Zinc(II) 5-(4-aminophenyl)-10,15,20-(tri-4-sulfonatophenyl)porphyrin triammonium (Zinc porphyrin) was covalently attached on gold nanoparticles (AuNPs) using a EDC/NHS coupling chemistry. In the first step, AuNPs were functionalized with 11-Mercaptoundecanoic acid (MUA) to introduce carboxylic groups. Briefly, 1 mL of MUA (100 μM) in 1:9 ethanol/water was added to 5 mL of citrate capped AuNPs (100 μg/mL). The solution was stirred overnight at room temperature under N_2 atmosphere. Later, the AuNPs were washed three times with water and centrifuged at 2500 rpm for 20 min to obtain MUA-capped AuNPs. In the second step, freshly prepared 1 mL EDC (100 mM) and 1 mL NHS (200 mM) was added to the MUA capped AuNPs to activate the carboxyl groups. The reaction was allowed to continue for 4 h under an N_2. Then, 1 mL of zinc porphyrin (100 μM) was added to this mixture and the solution was stirred at room temperature for 24 h

under dark. Finally, the AuNPs were washed 3-4 times with water and centrifuged at 2500 rpm for 20 min to obtain AuNPs conjugated with zinc porphyrin.

Cell Culture and Cell Experiments: A human glioblastoma cell line (U251s) was cultured and expanded under standard cell culture conditions, using culture medium (DMEM) supplemented with 10% fetal bovine serum (FBS) and 1% L-glutamine. The cells were passaged using trypsin, with all cells used in experiments having a passage number of <50. Cells were cultured onto microelectrode samples using Ibidi sticky slides® at 500,000 cells and left for 4-6 hours to attach before running EIS measurements. For EIS measurements sticky slides were removed, all traces of media were first washed away by submerging samples in deionized water and then 20 µl of electrolyte was added. During all experiments deionized water (18.2 MΩ) and sterile PBS (0.01M, ThermoFischer) was used.

For cellular uptake analysis, $1.5\times10_4$ U251 cells were seeded on 13 mm glass viewing area of a 35 mm glass-bottom dish (ThermoFisher SCIENTIFIC) and incubated at 37°C for 24 h. After 24 h, the culture medium was replaced with fresh medium containing 50 or 25 µg/ml AuNPs (functionalized with zinc porphyrin) for 6 or 24 h. After each incubation period, the media containing the AuNPs was removed and cells were washed thrice with PBS. The plasma membrane of the cells was stained using CellMask™ Green Plasma Membrane Stain (Thermo Fisher SCIENTIFIC) for 10 min. Later the cells were fixed with 4% formaldehyde for 5 min and subsequently washed 3 times with PBS. Afterward, cells were treated with DAPI for 5 min at RT under dark and washed again thrice with PBS. Finally, the cells were immersed in PBS and imaged using a Zeiss Elyra confocal microscope. Cellular uptake of AuNPs functionalized with zinc porphyrin was quantified by measuring fluorescent intensity of at least 20 different cells using ImageJ. The fluorescent intensity values were normalized to the total number of cells per field and expressed as corrected total cell fluorescence (CTCF) obtained by applying Equation 7.

$$CTCF = Integrated\ density - (Area\ of\ selected\ cell \times Mean\ fluorescence\ of\ background\ signal) \quad (7)$$

Supporting Information
Supporting Information is available from the Wiley Online Library or from the author.

Acknowledgements
This work was supported by the Engineering and Physical Sciences Research Council [Grant numbers EP/L015072/1 and EP/R004072/1]. The authors would like to thank Dominic Mosses, who performed some initial groundwork leading on to this study. Dr. Scott Young and Dr. Saul Vazquez-Reina are thanked for their assistance with ICP-MS analysis.

Received: ((will be filled in by the editorial staff))
Revised: ((will be filled in by the editorial staff))
Published online: ((will be filled in by the editorial staff))

References

[1] Mehrotra, P. Biosensors and their applications - A review. *J. Oral Biol. Craniofac. Res.* 6, 153–159 (**2016**).

[2] Rabaey, K. & Verstraete, W. Microbial fuel cells: Novel biotechnology for energy generation. *Trends Biotechnol.* 23, 291–298 (**2005**).

[3] Olofsson, P. S. & Tracey, K. J. Bioelectronic medicine: technology targeting molecular mechanisms for therapy. *J. Intern. Med.* 282, 3–4 (**2017**).

[4] Sanjuan-Alberte, P. et al. Wireless Nanobioelectronics for Electrical Intracellular Sensing. *ACS Appl. Nano Mater.* 2, 6397–6408 (**2019**).

[5] Fosdick, S. E., Knust, K. N., Scida, K. & Crooks, R. M. Bipolar electrochemistry. *Angew. Chemie* - Int. Ed. 52, 10438–10456 (**2013**).

[6] Loget, G., Zigah, D., Bouffier, L., Sojic, N. & Kuhn, A. Bipolar Electrochemistry: From Materials Science to Motion and Beyond. *Acc. Chem. Res*. 46, 2513–2523 (**2013**).

[7] Koefoed, L., Pedersen, S. U. & Daasbjerg, K. Bipolar Electrochemistry - A wireless approach for electrode reactions. *Curr. Opin. Electrochem*. 0–16 (**2017**).

[8] Karimian, N., Hashemi, P., Afkhami, A. & Bagheri, H. The principles of bipolar electrochemistry and its electroanalysis applications. *Curr. Opin. Electrochem*. (**2019**).

[9] Ellis, K. G. & Jansson, R. E. W. Further studies on the epoxidation of propylene in a bipolar trickle bed. *J. Appl. Electrochem*. 11, 531–535 (**1981**).

[10] Manji, A. & Oloman, C. W. Electrosynthesis of propylene oxide in a bipolar trickle-bed reactor. *J. Appl. Electrochem*. 17, 532–544 (**1987**).

[11] Lee, J. K., Shemilt, L. W. & Chun, H. S. Studies of bipolarity in fluidized bed electrodes. *J. Appl. Electrochem.* 19, 877–881 (**1989**).

[12] Backhurst, J. R., Coulson, J. M., Goodridge, F., Plimley, R. E. & Fleischmann, M. A Preliminary Investigation of Fluidized Bed Electrodes. *J. Electrochem. Soc.* 116, 1600 (**1969**).

[13] Smotkin, E. et al. Bipolar titanium dioxide/platinum semiconductor photoelectrodes and multielectrode arrays for unassisted photolytic water splitting. *J. Phys. Chem.* 90, 4604–4607 (**1986**).

[14] Cervera-March, S. et al. Modeling of Bipolar Semiconductor Photoelectrode Arrays for Electrolytic Processes. *J. Electrochem. Soc.* 135, 567 (**1988**).

[15] Wiesener, K., Ohms, D., Benczúr-Ürmössy, G., Berthold, M. & Haschka, F. High power metal hydride bipolar battery. *J. Power Sources* 84, 248–258 (**1999**).

[16] Loget, G. & Kuhn, A. Electric field-induced chemical locomotion of conducting objects. *Nat. Commun. 2,* 535–536 (**2011**).

[17] Perro, A., Reculusa, S., Ravaine, S., Bourgeat-Lami, E. & Duguet, E. Design and synthesis of Janus micro- and nanoparticles. *J. Mater. Chem.* 15, 3745 (**2005**).

[18] Loget, G., Roche, J. & Kuhn, A. True bulk synthesis of Janus objects by bipolar electrochemistry. *Adv. Mater.* 24, 5111–5116 (**2012**).

[19] Bradley, J. C., Crawford, J., Ernazarova, K., McGee, M. & Stephens, S. G. Wire formation on circuit boards using spatially coupled bipolar electrochemistry. *Adv. Mater.* 9, 1168–1171 (**1997**).

[20] Bradley, J.-C. et al. Creating electrical contacts between metal particles using directed electrochemical growth. *Nat.* 1997 3896648 389, 268–271 (**1997**).

[21] Loget, G. & Kuhn, A. Shaping and exploring the micro- and nanoworld using bipolar electrochemistry. *Anal. Bioanal. Chem.* 400, 1691–1704 (**2011**).

[22] Kusakabe, K., Morooka, S. & Kato, Y. Current paths and electrolysis efficiency in bipolar packed-bed electrodes. *J. Chem. Eng. Japan* 15, 45–50 (**1982**).

[23] Kusakabe, K., Morooka, S. & Kato, Y. Equivalent resistances for current pathways in a bipolar packed-bed electrode cell. *J. Chem. Eng. Japan* 19, 43–47 (**1986**).

[24] Sudoh, M., Kodera, T., Hino, H. & Shimamura, H. Oxidative Degradation Rate of Phenol in An Undivided Bipolar Electrolyzer. *J. Chem. Eng. Japan* 21, 536–538 (**1988**).

[25] Scida, K. et al. Fluorescence-Based Observation of Transient Electrochemical and Electrokinetic Effects at Nanoconfined Bipolar Electrodes. *ACS Appl. Mater. Interfaces* 11, 13777–13786 (**2019**).

[26] Macdonald, D. D. Reflections on the history of electrochemical impedance spectroscopy. *Electrochim. Acta* 51, 1376–1388 (**2006**).

[27] Epelboin, I., Keddam, M. & Takenouti, H. Use of impedance measurements for the determination of the instant rate of metal corrosion. *J. Appl. Electrochem.* 2, 71–79 (**1972**).

[28] Loveday, D., Peterspm, P. & Rodgers, B. Evalution of organic coatings with electrochemical impedance spectroscopy part 2: Application of EIS to coatings. CoatingsTech 1, 88–93 (**2004**).

[29] Chen, Z., He, C., Yu, F. & Wang, Y. Study and Application of Electrochemical Impedance Spectroscopy for Quickly Evaluating the Performance of Coatings and Predicting

the Failure Time in the Development of Waterborne Epoxy Micaceous Iron Oxide Coatings. *Int. J. Electrochem. Sci.* 12, 2798–2812 (**2017**).

[30] Selman, J. R. & Lin, Y. P. Application of ac impedance in fuel cell research and development. *Electrochim. Acta* 38, 2063–2073 (**1993**).

[31] Gomadam, P. M. & Weidner, J. W. Analysis of electrochemical impedance spectroscopy in proton exchange membrane fuel cells. *Int. J. Energy Res.* 29, 1133–1151 (**2005**).

[32] He, Z. & Mansfeld, F. Exploring the use of electrochemical impedance spectroscopy (EIS) in microbial fuel cell studies. *Energy Environ. Sci.* 2, 215–219 (**2009**).

[33] Blommaert, M. A., Vermaas, D. A., Izelaar, B., In'T Veen, B. & Smith, W. A. Electrochemical impedance spectroscopy as a performance indicator of water dissociation in bipolar membranes. *J. Mater. Chem. A* 7, 19060–19069 (**2019**).

[34] Randviir, E. P. & Banks, C. E. Electrochemical impedance spectroscopy: An overview of bioanalytical applications. *Anal. Methods* 5, 1098–1115 (**2013**).

[35] Kafka, J., Pänke, O., Abendroth, B. & Lisdat, F. A label-free DNA sensor based on impedance spectroscopy. *Electrochim. Acta* 53, 7467–7474 (**2008**).

[36] Kekomaki, S. et al. Successful treatment of platelet transfusion refractoriness: the use of platelet transfusions matched for both human leucocyte antigens (HLA) and human platelet alloantigens (HPA) in alloimmunized patients with leukaemia. *Eur. J. Haematol.* 60, 112–118 (**1998**).

[37] Bhardwaj, P., Rai, D. V., Garg, M. L. & Mohanty, B. P. Potential of electrical impedance spectroscopy to differentiate between healthy and osteopenic bone. *Clin. Biomech.* 57, 81–88 (**2018**).

[38] Yun, J. et al. Electrochemical impedance spectroscopy with interdigitated electrodes at the end of hypodermic needle for depth profiling of biotissues. *Sens. Actuators B Chem.* 237, 984–991 (**2016**).

[39] Yun, J., Hong, Y.-T., Hong, K.-H. & Lee, J.-H. Ex vivo identification of thyroid cancer tissue using electrical impedance spectroscopy on a needle. *Sens. Actuators B Chem.* 261, 537–544 (**2018**).

[40] Sun, T. & Morgan, H. Single-cell microfluidic Impedance cytometry: A review. *Microfluid. Nanofluid.* 8, 423–443 (**2010**).

[41] Lukic, S. & Wegener, J. Impedimetric Monitoring of Cell-Based Assays. In *eLS* 1–8 (**2015**).

[42] Cabuzu, D., Cirja, A., Puiu, R. & Grumezescu, A. Biomedical Applications of Gold Nanoparticles. *Curr. Top. Med. Chem.* 15, 1605–1613 (**2015**).

[43] Sanjuan-Alberte, P., Alexander, M. R., Hague, R. J. M. & Rawson, F. J. Electrochemically stimulating developments in bioelectronic medicine. *Bioelectron. Med.* 4, (**2018**).

[44] Sanjuan-Alberte, P. & Rawson, F. J. Engineering the spark into bioelectronic medicine. *Ther. Deliv.* 10, 139–142 (**2019**).

[45] Sanjuan-Alberte, P. et al. Remotely Controlled in Situ Growth of Silver Microwires Forming Bioelectronic Interfaces. *ACS Appl. Mater. Int.* 11, 8928–8936 (**2019**).

[46] Ostovari, M., Riahi Alam, N., Zabihzadeh, M., Gharib-Vand, M. M. & Hoseini-Ghahfarokhi, M. The effect of gold nanoparticles on electrical impedance of tissue on low frequency ranges. *J. Biomed. Phys. Eng.* 8, 241–250 (**2018**).

[47] Wegener, J., Keese, C. R. & Giaever, I. Electric cell-substrate impedance sensing (ECIS) as a noninvasive means to monitor the kinetics of cell spreading to artificial surfaces. *Exp. Cell Res.* 259, 158–166 (**2000**).

[48] What is ECIS? - Applied BioPhysics. Available at: https://www.biophysics.com/whatIsECIS.php. (Accessed: 9th March 2020)

[49] Gillis, K. D. Techniques for Membrane Capacitance Measurements. In *Single-Channel Recording* 155–198 (Springer US, **1995**).

[50] Majdoub, M. S., Maranganti, R. & Sharma, P. Understanding the origins of the intrinsic dead layer effect in nanocapacitors. *Phys. Rev. B - Condens. Matter Mater. Phys.* 79, (**2009**).

[51] Deng, Q., Liu, L. & Sharma, P. Flexoelectricity in soft materials and biological membranes. *J. Mech. Phys. Solids* 62, 209–227 (**2014**).

[52] Hart, F. X. & Palisano, J. R. The Application of Electric Fields in Biology and Medicine. In *Electric Field*, 161–186 (InTech, **2018**).

[53] Grimes, P. G., Bellows, R. J. & Zahn, M. Shunt Current Control in Electrochemical Systems Theoretical Analysis. In *Electrochemical Cell Design*, 259–292 (**1984**).

[54] Jiang, Y. et al. The Interplay of Size and Surface Functionality on the Cellular Uptake of Sub-10 nm Gold Nanoparticles. *ACS Nano* 9, 9986–9993 (**2015**).

.

Supporting Information

Impedimetric characterization of bioelectronic nano-antennae

Andie J. Robinson, Akhil Jain, Ruman Rahman, Sidahmed Abayzeed, Richard J. M. Hague, Frankie J. Rawson**

Nano BPEs

In order to further validate the theoretical framework outlined in Figure 2, impedance of systems with and without AuNP bipolar electrodes (BPEs) was measured in varying concentrations of electrolyte between deionized water and phosphate-buffered saline (PBS). Dilutions were made in 10 fold using a PBS stock (0.01 M Thermo Fischer). When looking at samples without BPEs, we saw no change in shape of the nyquist plot. All concentrations exhibiting a 45° slope which is characteristic of Warburg impedance due to diffusion limits. When BPEs are present we saw a change in the graphs shapes at high frequencies as you approach low PBS concentrations and deionized water. This semicircle that begins to form is due to a capacitance being introduced from the BPEs. This validates the theoretical framework showing that increasing impedance of electrolyte allows for increasing current driven though the BPEs shown by the increasing semicircle size.

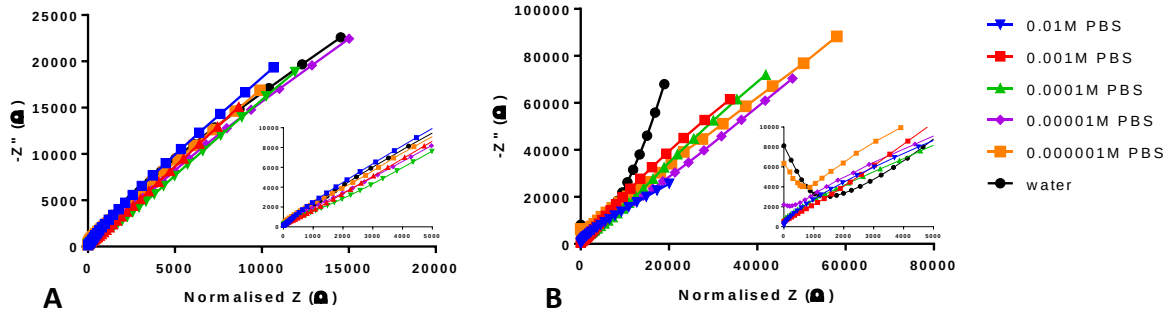

Figure S1: Varying PBS concentrations were tested in systems with (B) and without (A) AuNP bipolar electrodes. Real impedance was normalized to allow Nyquist plots to be overlayed. Insets show expanded lower frequency portion of graphs.

Circuits with the BPE component were first fitted to PBS data to determine if they were contributing to the impedance of the system due to current being driven though them. As seen in Figure S2, better fitting was produced by removing the BPE component, suggesting that no current is being driven through the BPEs.

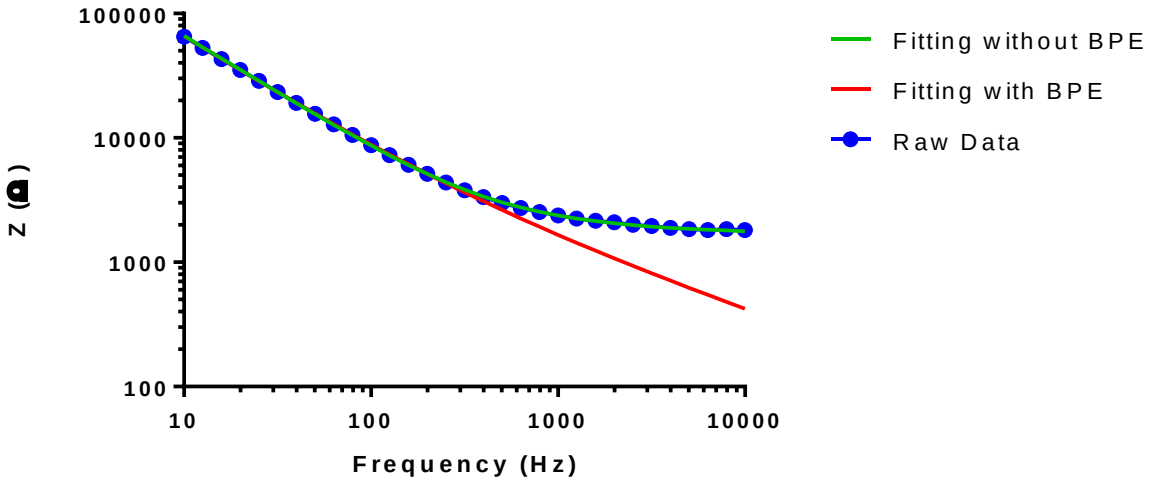

Figure S2: Raw data of bipolar system with AuNP BPEs in PBS. Fitting lines show fitting with (red) and without (green) the BPE component.

Cells with nano-BPEs

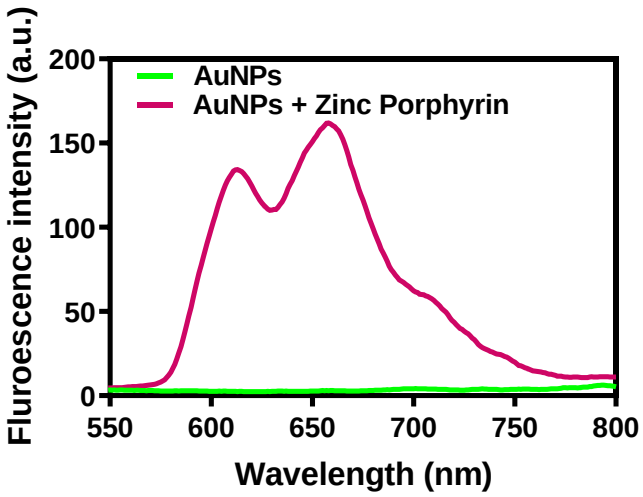

Figure S3. Fluorescent emission spectrum of AuNPs functionalized with zinc porphyrin monitored upon excitation with a wavelength of 422 nm.

To further study the cellular uptake of AuNPs, inductively coupled plasma mass spectroscopy (ICP-MS) was carried out (iCAPQ Thermo Fischer) with bare AuNPs. Using the same methods as described for confocal microscopy, ICP-MS samples were prepared by digesting samples in 5% aquaregia overnight, before then being diluted with milliQ water to reach a final acid concentration of 2%.[54] As seen in Figure S4, both cells (blue) and supernatant (red) were collected from incubation studies. Comparing concentrations, within the same time frame, it can be seen that the increase in Au is present in the supernatant and not the cells. This suggests that increasing concentration does not allow for increased cellular uptake within these conditions. There is however a significant difference between 6 and 24 hours of the same concentration. Au in cells increases, whilst Au in supernatant decreases, suggesting the increase in time allows for further cellular uptake from the supernatant. Due to both ICP-MS and confocal microscopy results, 50 μg/ml of AuNPs and an incubation time of 24 hours was used.

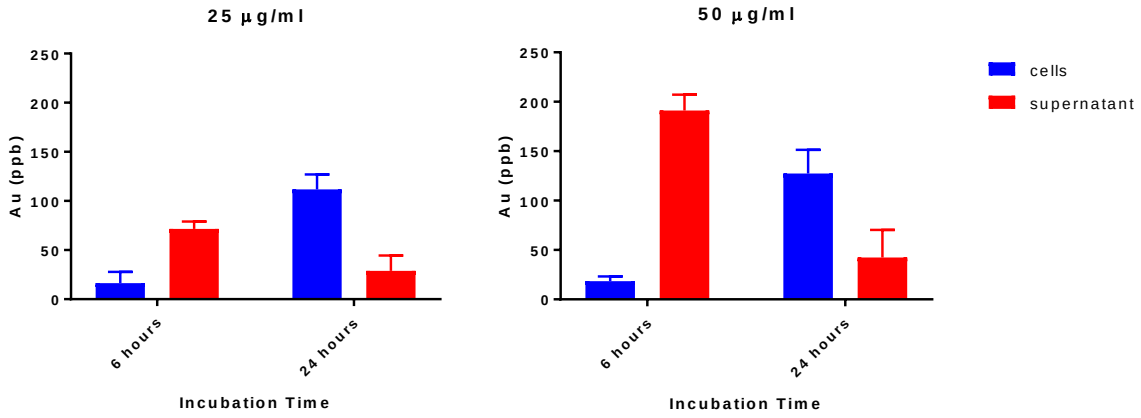

Figure S4. Inductively coupled plasma mass spectrometry (ICP-MS) results for 25 and 50 µg/ml of AuNPs incubated with U251 cells for 6 or 24 hours.

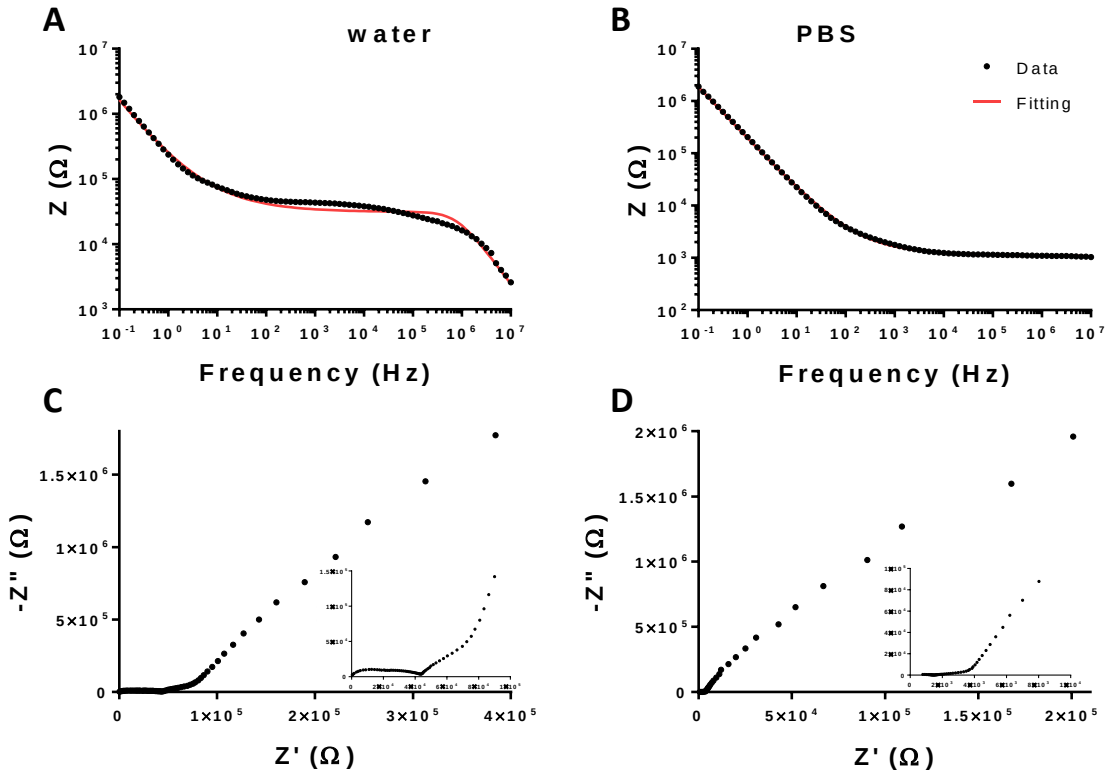

Figure S5. Graphs showing sample fitting of raw data of systems with living cells, in water (A) and PBS (B). Such fitting was used to determine resistance and capacitance values seen in Figure 7. Typical Nyquist plots for this data can be seen in C and D.

A